Letter

Microstructural Rearrangements in Triblock Polyelectrolyte Complex Hydrogels

Holly Senebandith, Fahed Albreiki, Phillip A. Kohl, Arthur Odenheimer, Khin C. Pyone, Youli Li, and Samanvaya Srivastava*

Read Online

ACCESS | Metrics & More | Article Recommendations | Supporting Information

Dehydrated Gel — PEC Hydrogel — Swollen or Rehydrated Hydrogels

−H$_2$O / +H$_2$O — PEC domains and PEO matrix hydrate — +H$_2$O — PEO matrix expands — Equilibration — PEC domain fission and rearrangements
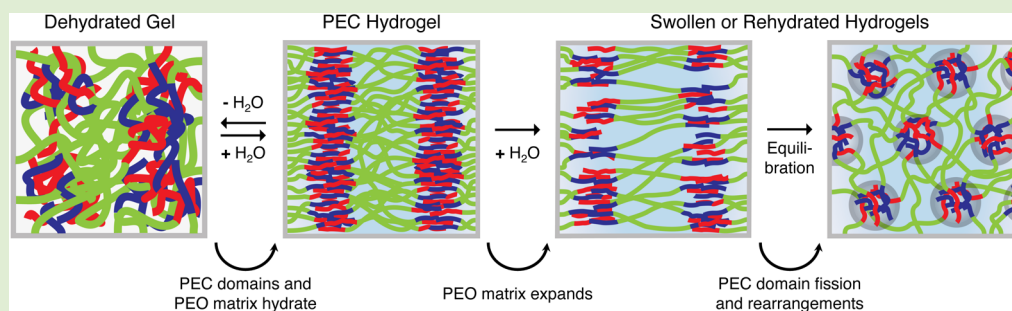
ABSTRACT: We examine the swelling and dehydration−rehydration response of triblock polyelectrolyte complex (PEC) hydrogels using small-angle X-ray scattering and rheology to demonstrate that PEC hydrogel microstructures equilibrate readily into morphologies corresponding to *pristine* PEC hydrogels with comparable polymer contents. As such, we show that PEC hydrogels possess identical microstructures independent of the route employed to make them. We propose PEC domain fission as the dominant mechanism for these microstructural rearrangements. Furthermore, we show that mixing two fully formed PEC hydrogels with distinct microstructures leads to microstructural rearrangements, resulting in hydrogels with intermediate microstructure and viscoelastic properties of the individual PEC hydrogels. Our findings provide explicit experimental proof that PEC hydrogel microstructures are not kinetically trapped and have implications for their processing in diverse applications.

The unique features associated with self-assembled polyelectrolyte complex (PEC) hydrogels, like swift self-assembly, rapid viscoelastic recovery after deformation, and reversible complexation,[1−5] emerge from a well-studied phenomenon involving the liquid−liquid phase separation of aqueous solutions of oppositely charged macromolecules such as polyelectrolytes, proteins, and macroions.[3,6−10] Block polyelectrolyte (bPE) architectures facilitate the arrest of the phase separation at the nanoscale, resulting in the formation of nanoscale PEC domains embedded in self-assembled networks. Thus, oppositely charged bPEs form a rich diversity of three-dimensional networks with hierarchical microstructures.[11] Significant recent progress has accomplished an improved understanding of the microstructural diversity and bulk properties (e.g., tunable viscoelastic response, response to stimuli, and controlled swelling characteristics[5,6,9,12,13]) of PEC hydrogels and also explored their utility as (bio)inks for additive manufacturing,[14,15] scaffolds,[9,16,17] and drug carriers.[5,18] Yet, one question regarding PEC hydrogels remains persistently unanswered − do the PEC hydrogel microstructures represent equilibrium or kinetically trapped structures?

PEC hydrogels have been shown, both in experiments[1,6,11,12,19,20] and theoretical[21,22] investigations, to exhibit microphase separation resulting in distinct PEC domains arranged in diverse morphologies, including disordered spheres, body-centered cubic arrangements of spheres, hexagonally close-packed cylinders, and parallel stacked lamellae. The morphology of the PEC domains in PEC hydrogels has been shown to depend on polymer block lengths, polymer concentration, salt concentration, pH, and temperature.[1,6,8,11,12,19,20,23−25] Moreover, the microstructure directly influences the rheological behavior (i.e., shear moduli) of PEC hydrogels,[6,11] which, in turn, has direct consequences on their performance during extrusion, printing, processing, and long-term storage.[14,15]

Theoretical studies[21,22] have indicated that PEC hydrogels are equilibrium self-assemblies. However, these theoretical efforts have also noted the coexistence of PEC domain morphologies near the morphology transition boundaries,

attributed to a shallow free energy landscape.[21] Correspondingly, experimental studies have noted coexisting morphologies in PEC hydrogels. Still, it is not clear yet if those coexisting morphologies appear owing to nonequilibrated assemblies or are representative of equilibrated structures.[6,11,19−21]

In this Letter, we test the hypothesis that self-assembled PEC hydrogels are equilibrium structures, which are expected to arrive at the same microstructure independent of the route employed to make the hydrogel through a series of experiments seeking to probe the dehydration and swelling response of PEC hydrogels. We formulated PEC hydrogels as follows: (i) mixing aqueous solutions of oppositely charged bPEs in appropriate ratio to form *pristine* PEC hydrogels, (ii) controlled swelling from a concentrated PEC hydrogel to form *swollen* PEC hydrogels, and (iii) complete dehydration followed by controlled rehydration to form *rehydrated* PEC hydrogels. In all three cases, bPE concentration in the hydrogels was precisely controlled, and small-angle X-ray scattering (SAXS) was utilized to characterize and compare their microstructures. At the same time, the shear moduli were measured to contrast their rheological behavior. We also pursued the mixing of preformed hydrogels with distinct microstructures, postulating that if the PEC hydrogels are equilibrated structures, then the resultant *mixed* hydrogel should possess an intermediate, uniform microstructure rather than a microstructure comprising mixed morphologies. Concomitantly, we note that understanding the responses of PEC hydrogels to varied processing operations (such as mixing, swelling, and dehydration) should have significant implications on their developing utility as functional biomaterials (e.g., reconstitution of dried hydrogel bandages, synthetic biological membranes, and drug release vehicles), contributing to the practical significance of this study.

We began by investigating the microstructural evolution of PEC hydrogels upon their controlled swelling. PEC hydrogels were made at a high bPE concentration C_{bPE} and then diluted with predetermined volumes of water to a lower C_{bPE}. If the PEC hydrogel microstructures were equilibrium structures, we expected a microstructural transition as water was added to swell the hydrogels. In contrast, if these PEC hydrogels did not possess an equilibrium microstructure and instead comprised kinetically trapped assemblies, we expected them to swell yet retain their original microstructure.

SAXS experiments confirmed microstructural rearrangements in *swollen* PEC hydrogels. PEC hydrogels comprising oppositely charged triblock polyelectrolytes (ammonium and sulfonate functionalized poly(allyl glycidyl ether)$_{119}$ - poly-(ethylene oxide)$_{454}$ - poly(allyl glycidyl ether)$_{119}$; a+sPAGE$_{119}$-PEO$_{454}$-PAGE$_{119}$; Figure S1) were prepared at C_{bPE} = 50 wt % and controllably swollen to 40, 30, and 20 wt % (Figure 1a). SAXS spectra of the *pristine* 50 wt % hydrogel (top gray trace in Figure 1b) revealed parallelly stacked PEC lamellae (LAM), characterized by the appearance of secondary Bragg peaks at $2q^*$ and $3q^*$, with q^* being the wave vector position of the primary Bragg peak (see also Figure S2). These observations are in agreement with reports in the literature for similar systems.[11] As the hydrogel swelled from 50 wt % to 40 wt %, we observed a leftward shift and a broadening of the primary scattering peak. Importantly, the SAXS spectrum for the *swollen* 40 wt % PEC hydrogel (blue traces in Figure 1b) was nearly identical to the *pristine* PEC hydrogel (gray traces in Figure 1b) prepared by mixing aqueous solutions of the oppositely charged bPEs at C_{bPE} = 40 wt %. Dilution to C_{bPE} =
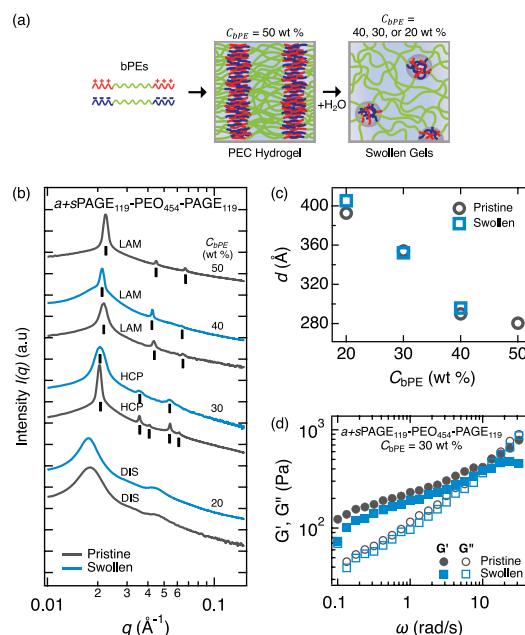

Figure 1. Swelling experiments in a+sPAGE$_{119}$-PEO$_{454}$-PAGE$_{119}$ PEC hydrogels. (a) PEC hydrogels (C_{bPE} = 50 wt %) were swollen to lower C_{bPE} by adding controlled amounts of water. (b) Scattering intensity, $I(q)$, as a function of wave vector, q, for *pristine* (gray) and *swollen* (blue) gels. Spectra are arbitrarily shifted vertically for clarity. Black vertical bars indicate assigned Bragg peaks. DIS, HCP, and LAM correspond to disordered spheres, hexagonally close-packed cylinders, and lamellae morphologies of PEC domains. (c) Characteristic spacing, d, as a function of C_{bPE} for *pristine* (gray) and *swollen* (blue) hydrogels. (d) Frequency sweep results showing storage, G', and loss, G'', moduli of *pristine* (gray) and *swollen* (blue) hydrogels at C_{bPE} = 30 wt %, measured in the frequency range of ω = 0.1 to 40 rad/s at a strain of γ = 0.1%.

30 wt % led to a further leftward shift and broadening of the primary scattering peak and a microstructural transition to hexagonally close-packed PEC cylinders (HCP), indicated by the appearance of the secondary Bragg peaks at $2q^*$, $\sqrt{7}q^*$, and $3q^*$ (see Table S1 for complete peak assignments, see also Figure S2). Notably, the secondary Bragg peaks disappeared for the *swollen* C_{bPE} = 20 wt % hydrogels, and the primary scattering peak broadened considerably and continued to shift to lower q, revealing reduced microstructural correlation and an order−disorder transition, with the spectrum corresponding to a disordered, strongly correlated assembly of spherical PEC domains (DIS). Again, the spectra of the *swollen* and the *pristine* hydrogels were identical. We also confirmed similar trends in a+sPAGE$_{49}$-PEO$_{454}$-PAGE$_{49}$ hydrogels (Figure S3 and Table S2), wherein *swollen* hydrogels exhibited similar SAXS spectra to *pristine* hydrogels at identical C_{bPE}, indicating that this microstructural evolution is not restricted to bPEs with long end blocks.

Modeling of the SAXS spectra enabled quantitative microstructural comparisons between *swollen* and *pristine* hydrogels. Figure 1c summarizes the characteristic spacing d (which corresponds to the center-to-center distance, interaxial distance, and layer repeat distance for the DIS, HCP, and LAM microstructures, respectively) of the two hydrogel families as a function of C_{bPE}. Evidently, both preparation methods resulted in nearly identical characteristic spacings for all concentrations. We note that the small C_{bPE} span limits any

d-C_{bPE} scaling predictions, although tentatively, we observe a $d \sim C_{bPE}^{-1/3}$ dependence (Figure S4).

Modeling of the PEC domains as spheres and cylinders for the DIS and HCP microstructures, respectively, showed strong similarities in microstructure (see Materials and Methods in the Supporting Information for details on the fitting). The radius of the spherical PEC domains in the DIS microstructure was 13.3 and 13.7 nm for the *pristine* and *swollen* hydrogels (C_{bPE} = 20 wt %), respectively (Figure S5). Similarly, the radius of the cylindrical PEC domains in the HCP microstructure was 9.8 and 10.1 nm for the *pristine* and *swollen* hydrogels (C_{bPE} = 30 wt %), respectively. The similarity in domain radii between 30 and 20 wt % gels supports a domain fission mechanism of equilibration during hydrogel swelling.

The shear moduli G' and G'' of the *swollen* and *pristine* hydrogels, measured by subjecting the hydrogels to a small amplitude oscillatory strain (γ = 0.1%), were identical as well, providing evidence of the similarity of not only the microstructure but also of the bulk response to deformation between the *pristine* and *swollen* hydrogels. Figure 1d shows G' and G'' as a function of angular frequency ω for a+sPAGE$_{119}$-PEO$_{454}$-PAGE$_{119}$ hydrogels at C_{bPE} = 30 wt %, indicating the solid-like behavior of both hydrogels at low ω and a G' - G'' crossover around the same $\omega \sim 15$ rad/s for both hydrogels, indicating similar viscoelastic behavior.

In an attempt to probe the role of water in avoiding kinetic trapping of the self-assembled structures, the swelling experiments were pushed to the extreme by starting with completely dehydrated PEC hydrogels. As such, PEC hydrogels were formulated, dehydrated completely by lyophilization, and systematically rehydrated to form a series of *rehydrated* PEC hydrogels with known C_{bPE} (Figure 2a). Again, we hypothesized that if the PEC hydrogels were kinetically trapped, the *rehydrated* gels must possess the same microstructure as the starting hydrogel (*pristine* gel with C_{bPE} = 50 wt %).

All *rehydrated* PEC hydrogels comprising a+sPAGE$_{119}$-PEO$_{454}$-PAGE$_{119}$ exhibited a similar microstructure compared to their corresponding *pristine* gels (Figure 2b). The *rehydrated* gels were prepared by completely dehydrating a 50 wt % gel followed by rehydration with a calculated amount of water. Expectedly,[11] the 20 wt % gels, both *rehydrated* (blue traces in Figure 2b) and *pristine* (gray traces in Figure 2b), exhibited the DIS microstructure. A disorder–order transition to HCP was noted for both the *rehydrated* and *pristine* gels at C_{bPE} = 30 wt %; the Bragg peaks for the *rehydrated* gels corresponded to $2q^*$ and $\sqrt{7}q^*$ while those for the *pristine* gels corresponded to $\sqrt{3}q^*$, $2q^*$, $\sqrt{7}q^*$, and $3q^*$ (see also Figure S2; see Table S3 for complete peak assignments). We also observe peak splitting in the *rehydrated* gel at C_{bPE} = 30 wt %, indicating coexisting microstructures of different spacing. Additionally, an order–order transition from HCP to LAM morphology was observed at C_{bPE} = 40 wt % (Bragg peaks for the *rehydrated* and the *pristine* hydrogels corresponded to $2q^*$ and $3q^*$). These disorder–order and order–order transitions, noted in both the *pristine* and the *rehydrated* gels, were consistent with previous reports.[11] We verified similar microstructural progressions in hydrogels comprising shorter end-blocks, a+sPAGE$_{49}$-PEO$_{454}$-PAGE$_{49}$ (Figure S6 and Table S4), again demonstrating that this microstructural evolution is not restricted to bPEs with long end-blocks. Additionally, this behavior was consistently witnessed at other starting C_{bPE} (Figure S7 and Figure S8) and in hydrogels with an entirely different cationic charge
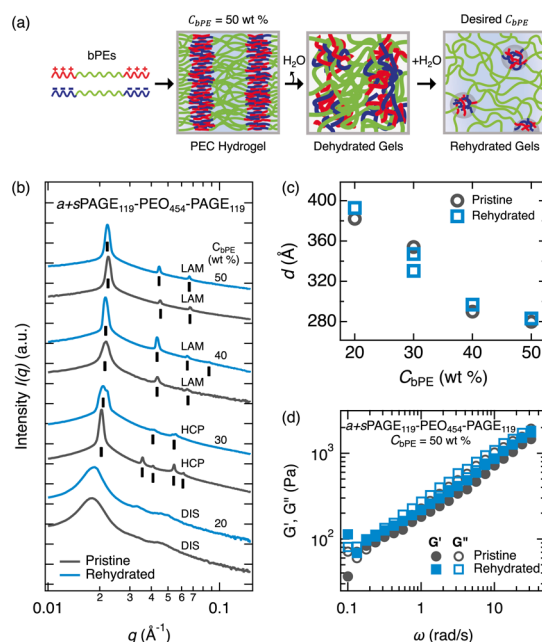

Figure 2. Dehydration and rehydration experiments in a+sPAGE$_{119}$-PEO$_{454}$-PAGE$_{119}$ PEC hydrogels. (a) Concentrated hydrogels were prepared at C_{bPE} = 50 wt %, dehydrated completely, and then rehydrated with water. (b) $I(q)$ spectra for *pristine* (gray) and *rehydrated* (blue) gels plotted as a function of q. Spectra are arbitrarily shifted vertically for clarity. Black vertical bars indicate assigned Bragg peaks. DIS, HCP, and LAM correspond to disordered spheres, hexagonally close-packed cylinders, and lamellae morphologies of PEC domains. (c) Characteristic spacing, d, as a function of C_{bPE} from modeling of the SAXS profiles plotted in (b). (d) Frequency sweep results showing storage G' and loss G'' moduli of *pristine* (gray) and *rehydrated* (blue) hydrogels, measured in the frequency range of ω = 0.1 to 40 rad/s at a strain of γ = 0.1%.

functional group (guanidinium, Figure S9). These results provided additional confirmation of the equilibration of PEC hydrogels and showcased that rearrangements are agnostic to starting C_{bPE}, charge functional group (guanidinium or ammonium), and end-block length.

Moreover, the PEC domain sizes and spacings for the *pristine* and the *rehydrated* gels were similar and followed trends consistent with previous reports.[11,13] Spacings corresponding to the fitted q^* Bragg peaks are plotted in Figure 2c and highlight the similarity in d-spacings between *rehydrated* and *pristine* samples, which also agree well with the d-spacings for the *swollen* samples shown in Figure 1. Of note, we report two different spacings of HCP microstructure for the *rehydrated* gel at C_{bPE} = 30 wt %, a result of peak-splitting in the SAXS spectrum (Figure 2b), which is predicted due to a shallow free energy landscape driving the assembly of these materials.[21] As with the *swollen* hydrogels, the size of the PEC domains of the *rehydrated* hydrogels is similar to their *pristine* counterparts, with a spherical radius of 13.5 nm for *rehydrated* gels (compared to 13.2 nm for *pristine* gels) at C_{bPE} = 20 wt %, and a cylindrical radius of 10.1 nm for *rehydrated* gels (compared to 10.1 nm for *pristine* gels) at C_{bPE} = 30 wt % (Figure S10). Again, the similarity in domain radii upon microstructural changes supports an equilibration mechanism via domain fission.

Shear rheology measurements further substantiated the similar bulk properties of the hydrogel pairs. Figure 2d shows unchanged shear moduli (G' and G'') among *pristine*
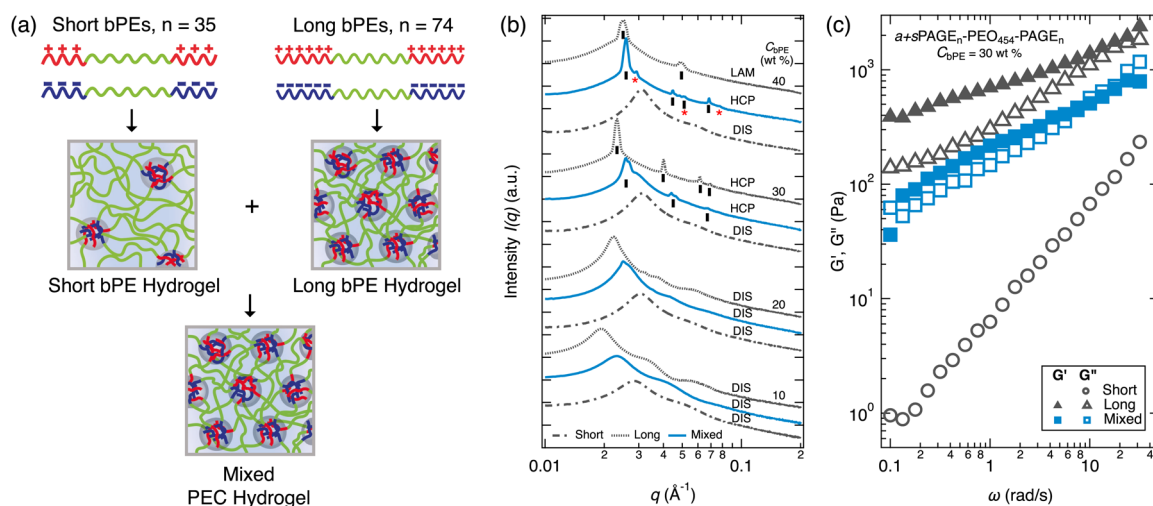
Figure 3. *Mixed* $a+s\text{PAGE}_{35}\text{-PEO}_{454}\text{-PAGE}_{35}$ + $a+s\text{PAGE}_{74}\text{-PEO}_{454}\text{-PAGE}_{74}$ PEC hydrogels. (a) Short bPE hydrogels were formulated with short-length bPEs, $a+s\text{PAGE}_{35}\text{-PEO}_{454}\text{-PAGE}_{35}$. Separately, long bPE hydrogels were formulated with long-length bPEs, $a+s\text{PAGE}_{74}\text{-PEO}_{454}\text{-PAGE}_{74}$. The short bPE hydrogels and long bPE hydrogels of the same C_{bPE} were mixed in a 1:1 ratio to yield *mixed* PEC hydrogels. Schematic is shown for the gels at C_{bPE} = 30 wt %. (b) SAXS spectra plotted as $I(q)$ versus q. The spectra for short bPE gels, long bPE gels, and *mixed* gels are depicted by dash-dot, dot, and solid lines. Black vertical bars and red asterisks indicate the primary and secondary set of Bragg peaks, respectively. DIS, HCP, and LAM correspond to disordered spheres, hexagonally close-packed cylinders, and lamellae morphologies of PEC domains. Spectra have been vertically shifted arbitrarily for clarity. (c) Frequency sweep results for *pristine* short bPE hydrogel (gray circles), *pristine* long bPE hydrogel (gray triangles), and *mixed* hydrogel (blue squares); samples are C_{bPE} = 30 wt %.
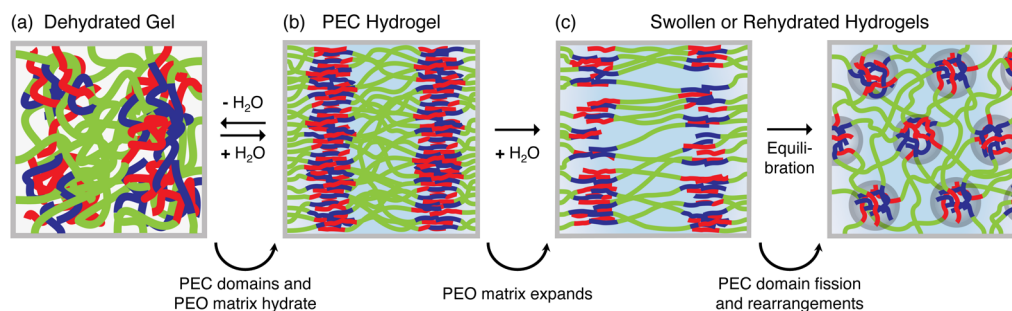

Figure 4. Proposed mechanism of microstructural rearrangements. (a) Water added to dehydrated gels partitions into both the PEC domains (finitely) and the PEO matrix during the initial rehydration of the (b) PEC hydrogel. (c) Additional water added to the PEC hydrogel can partition only into the PEO matrix, causing gel swelling and PEO chain expansion, resulting in PEC domain fission and order–order and order–disorder transformations in *swollen* or *rehydrated* hydrogels during equilibration.

and *rehydrated* $a+s\text{PAGE}_{119}\text{-PEO}_{454}\text{-PAGE}_{119}$ gels. Likewise, comparable shear moduli were also noted for *pristine* and *rehydrated* gels comprised of guanidinium and sulfonate functionalized $\text{PAGE}_{51}\text{-PEO}_{454}\text{-PAGE}_{51}$ and for $a+s\text{PAGE}_{119}\text{-PEO}_{454}\text{-PAGE}_{119}$ and $a+s\text{PAGE}_{49}\text{-PEO}_{454}\text{-PAGE}_{49}$ gels rehydrated to C_{bPE} = 30 wt % (Figure S11). Taken together with the microstructure results, our data shows that the hydrogel microstructure is pathway-independent and, thus, not kinetically trapped.

As a final route to test our hypothesis that PEC hydrogels are equilibrium assemblies, we performed mixing experiments where PEC hydrogels comprising bPEs with different charged block lengths ($a+s\text{PAGE}_{35}\text{-PEO}_{454}\text{-PAGE}_{35}$ and $a+s\text{PAGE}_{74}\text{-PEO}_{454}\text{-PAGE}_{74}$), and thus, distinct microstructures, were formulated as separate gels. Subsequently, the individual short-bPE and long-bPE hydrogels were mixed in a 1:1 ratio (Figure 3a). If the gels were equilibrium structures, we expected to see a homogeneous microstructure in the *mixed* gels. In contrast, if they were kinetically trapped assemblies, we expected to see a heterogeneous mix of distinct microstructures in the *mixed* gels.

Mixed PEC hydrogels exhibited homogeneous microstructures of intermediate length scale and morphology (Figure 3b; see also Figure S2). Notably, the 40 wt % *mixed* gel (top blue trace in Figure 3b) displayed HCP microstructure with a split primary peak; Bragg peaks were noted at $\sqrt{3}\,q^*$, $\sqrt{4}\,q^*$, $\sqrt{7}\,q^*$, with an additional set of peaks at $\sqrt{3}\,q^\dagger$ and $\sqrt{7}\,q^\dagger$, with $q^\dagger \sim 0.029$ Å^{-1} being the location of the second primary peak (the second set of peaks are denoted with red asterisks in Figure 3b). The corresponding short end-block and long end-block bPE *pristine* gels were classified as DIS (dash-dotted traces in Figure 3b) and LAM (dotted traces in Figure 3b; secondary Bragg peak assigned at $2q^*$), respectively. Interestingly, the *mixed* gel at C_{bPE} = 30 wt % was characterized as HCP (Bragg peaks at $\sqrt{3}\,q^*$ and $\sqrt{7}\,q^*$), but it displayed broadening in q^* similar to the single correlation peak of a DIS gel and splitting in the $\sqrt{3}\,q^*$ secondary peak indicative of a mixed morphology (second to top blue trace in Figure 3b). Both *mixed* and *pristine* gels at C_{bPE} = 10 and 20 wt % exhibited DIS microstructure. All *mixed* spectra matched their *pristine* counterparts, which were formed by combining aqueous

solutions of aPAGE$_{35}$-PEO$_{454}$-PAGE$_{35}$, aPAGE$_{74}$-PEO$_{454}$-PAGE$_{74}$, sPAGE$_{35}$-PEO$_{454}$-PAGE$_{35}$, and sPAGE$_{74}$-PEO$_{454}$-PAGE$_{74}$ at C_{bPE} = 10, 20, 30, and 40 wt % (Figure S12). Complete Bragg peak assignments can be found in Tables S5 and S6. Again, we attribute the coexisting microstructures to the shallow energy landscape driving the assembly of these materials.[21]

The domain spacing of the *mixed* gels was found to be intermediate to the domain spacing for their corresponding short-bPE and long-bPE *pristine* gels. Likewise, the spherical PEC domains also revealed intermediate domain radii. For *mixed* gels at C_{bPE} = 10 and 20 wt %, the radii were ∼8 nm, which represented intermediate domain sizes between both short-bPE (∼6 nm) and long-bPE (∼10 nm) *pristine* gels at both concentrations (Figure S13). Likewise, rheological measurements confirmed that the intermediate microstructures of the *mixed* gels resulted in intermediate moduli (Figure 3c), demonstrating the tunable shear properties achievable via *mixed* gels.

We propose the fission of PEC domains as the primary mechanism responsible for the microstructural rearrangements in PEC hydrogels, as illustrated in Figure 4. During the swelling of a dehydrated PEC hydrogel (SAXS spectrum shown in Figure S14), water is absorbed into both the PEO matrix and the PEC domains during the initial rehydration. The PEC domains only rehydrate until equilibrium is attained according to the bPE block length. Additional water partitions into the PEO matrix of the PEC hydrogel. We note that similar behavior was seen in bulk coacervate systems in equilibrium with their supernatant phase, where the introduction of excess supernatant did not influence the volume of the complex phase (Figure S15). This additional water causes PEO chain stretching and domain fission, where the domains break apart and reform into the energetically most favorable configuration based on the new composition of the hydrogel (Figure 4). We note that the stretching of the PEO chains has been shown previously to dictate PEC domain morphology,[11,20] and core fission has been demonstrated as an equilibration mechanism in amphiphilic block copolymer assemblies[26,27] and in polyelectrolyte micellar assemblies.[28] This model is supported by SAXS modeling[29] (Figure S5 and Figure S10), as the radii of the PEC domains remain nearly constant in each phase despite continual growth in the characteristic spacing with increasing water content.

In summary, we present controlled swelling and dehydration−rehydration experiments to establish that PEC hydrogels are equilibrium structures. Furthermore, the microstructures of *swollen* and *rehydrated* hydrogels matched their *pristine* counterparts. These data directly show that PEC hydrogel microstructures are not kinetically trapped, hereby experimentally resolving a decade-long assumption made on the state of PEC hydrogel microstructures.[6,11,19−21] We also demonstrate that microstructural rearrangements occur when two preformed PEC hydrogels with distinct microstructures are mixed, leading to intermediate microstructures and shear moduli. Lastly, we proposed a simple mechanism to explain the microstructural rearrangements. We anticipate that these results will be vital for implementing PEC hydrogels in future applications, informing the long-term storage, transportation state, and reconstitution conditions required to maintain the desired PEC hydrogel microstructures and properties.

■ ASSOCIATED CONTENT

Ⓢ Supporting Information

The Supporting Information is available free of charge at https://pubs.acs.org/doi/10.1021/acsmacrolett.5c00029.

Materials and methods, Bragg peak assignments, SAXS spectra for PEC hydrogels, SAXS spectra fits, power-law fits, frequency sweeps showing shear moduli (G' and G'') as a function of angular frequency (ω) for PEC hydrogels, bulk complex coacervate experiment (PDF)

■ AUTHOR INFORMATION

Corresponding Author

Samanvaya Srivastava − *Department of Chemical and Biomolecular Engineering, University of California, Los Angeles, Los Angeles, California 90095, United States; BioPACIFIC Materials Innovation Platform, California NanoSystems Institute, and Institute for Carbon Management, University of California, Los Angeles, Los Angeles, California 90095, United States;* ⓘ orcid.org/0000-0002-3519-7224; Email: samsri@ucla.edu

Authors

Holly Senebandith − *Department of Chemical and Biomolecular Engineering, University of California, Los Angeles, Los Angeles, California 90095, United States; Department of Chemistry and Biochemistry and BioPACIFIC Materials Innovation Platform, University of California, Los Angeles, Los Angeles, California 90095, United States;* ⓘ orcid.org/0000-0002-9076-8667

Fahed Albreiki − *Department of Chemical and Biomolecular Engineering, University of California, Los Angeles, Los Angeles, California 90095, United States; BioPACIFIC Materials Innovation Platform, University of California, Los Angeles, Los Angeles, California 90095, United States*

Phillip A. Kohl − *Materials Research Laboratory and BioPACIFIC Materials Innovation Platform, University of California, Santa Barbara, Santa Barbara, California 93106, United States*

Arthur Odenheimer − *Department of Chemical and Biomolecular Engineering, University of California, Los Angeles, Los Angeles, California 90095, United States; Department of Chemistry and Biochemistry, University of California, Los Angeles, Los Angeles, California 90095, United States*

Khin C. Pyone − *Department of Chemical and Biomolecular Engineering, University of California, Los Angeles, Los Angeles, California 90095, United States*

Youli Li − *Materials Research Laboratory and BioPACIFIC Materials Innovation Platform, University of California, Santa Barbara, Santa Barbara, California 93106, United States;* ⓘ orcid.org/0000-0001-5117-3874

Complete contact information is available at:
https://pubs.acs.org/10.1021/acsmacrolett.5c00029

■ REFERENCES

(1) Kim, J.-M.; Heo, T.-Y.; Choi, S.-H. Structure and Relaxation Dynamics for Complex Coacervate Hydrogels Formed by ABA Triblock Copolymers. *Macromolecules* **2020**, *53* (21), 9234−9243.

(2) Sun, Y.; Deming, T. J. Self-Healing Multiblock Copolypeptide Hydrogels via Polyion Complexation. *ACS Macro Lett.* **2019**, *8* (5), 553−557.

(3) Wei, S.-C.; Pan, M.; Li, K.; Wang, S.; Zhang, J.; Su, C.-Y. A Multistimuli-Responsive Photochromic Metal-Organic Gel. *Adv. Mater.* **2014**, *26* (13), 2072−2077.

(4) Wu, B.; Lewis, R. W.; Li, G.; Gao, Y.; Fan, B.; Klemm, B.; Huang, J.; Wang, J.; Cohen Stuart, M. A.; Eelkema, R. Chemical Signal Regulated Injectable Coacervate Hydrogels. *Chem. Sci.* **2023**, *14* (6), 1512−1523.

(5) Ishii, S.; Kaneko, J.; Nagasaki, Y. Dual Stimuli-Responsive Redox-Active Injectable Gel by Polyion Complex Based Flower Micelles for Biomedical Applications. *Macromolecules* **2015**, *48* (9), 3088−3094.

(6) Krogstad, D. V.; Lynd, N. A.; Choi, S.-H.; Spruell, J. M.; Hawker, C. J.; Kramer, E. J.; Tirrell, M. V. Effects of Polymer and Salt Concentration on the Structure and Properties of Triblock Copolymer Coacervate Hydrogels. *Macromolecules* **2013**, *46* (4), 1512−1518.

(7) Srivastava, S.; Tirrell, M. V. Polyelectrolyte Complexation. In *Advances in Chemical Physics*; Rice, S. A., Dinner, A. R., Eds.; John Wiley & Sons, Inc., 2016; *161*, pp 499−544.

(8) Lemmers, M.; Sprakel, J.; Voets, I. K.; van der Gucht, J.; Cohen Stuart, M. A. Multiresponsive Reversible Gels Based on Charge-Driven Assembly. *Angew. Chem., Int. Ed.* **2010**, *49* (4), 708−711.

(9) Cui, H.; Zhuang, X.; He, C.; Wei, Y.; Chen, X. High Performance and Reversible Ionic Polypeptide Hydrogel Based on Charge-Driven Assembly for Biomedical Applications. *Acta Biomaterialia* **2015**, *11*, 183−190.

(10) Chen, S.; Wang, Z.-G. Driving Force and Pathway in Polyelectrolyte Complex Coacervation. *Proc. Natl. Acad. Sci. U.S.A.* **2022**, *119* (36), No. e2209975119.

(11) Srivastava, S.; Levi, A. E.; Goldfeld, D. J.; Tirrell, M. V. Structure, Morphology, and Rheology of Polyelectrolyte Complex Hydrogels Formed by Self-Assembly of Oppositely Charged Triblock Polyelectrolytes. *Macromolecules* **2020**, *53* (14), 5763−5774.

(12) Hunt, J. N.; Feldman, K. E.; Lynd, N. A.; Deek, J.; Campos, L. M.; Spruell, J. M.; Hernandez, B. M.; Kramer, E. J.; Hawker, C. J. Tunable, High Modulus Hydrogels Driven by Ionic Coacervation. *Adv. Mater.* **2011**, *23* (20), 2327−2331.

(13) Li, D.; Göckler, T.; Schepers, U.; Srivastava, S. Polyelectrolyte Complex-Covalent Interpenetrating Polymer Network Hydrogels. *Macromolecules* **2022**, *55* (11), 4481−4491.

(14) Göckler, T.; Li, D.; Grimm, A.; Mecklenburg, F.; Grün, M.; Schepers, U.; Srivastava, S. Polyelectrolyte Complex Hydrogel Scaffoldings Enable Extrusion-Based 3D Bioprinting of Low-Viscosity Bioinks. October 13, 2023; *Chemrxiv*, 2023. DOI: 10.26434/chemrxiv-2023-v2tx2-v2.

(15) Göckler, T.; Albreiki, F.; Li, D.; Grimm, A.; Mecklenburg, F.; Urueña, J. M.; Schepers, U.; Srivastava, S. Block Polyelectrolyte Additives That Modulate the Viscoelasticity and Enhance the Printability of Gelatin Inks at Physiological Temperatures. *ACS Appl. Polym. Mater.* **2024**, *6* (5), 2427−2441.

(16) Li, D.; Ghovvati, M.; Annabi, N.; Srivastava, S. Polyelectrolyte Complex Scaffoldings for Photocrosslinked Hydrogels. *Mol. Syst. Des. Eng.* **2023**, *8*, 611−623.

(17) Nguyen, D. H. T.; Utama, R. H.; Tjandra, K. C.; Suwannakot, P.; Du, E. Y.; Kavallaris, M.; Tilley, R. D.; Gooding, J. J. Tuning the Mechanical Properties of Multiarm RAFT-Based Block Copolyelectrolyte Hydrogels via Ionic Cross-Linking for 3D Cell Cultures. *Biomacromolecules* **2023**, *24* (1), 57−68.

(18) Lee, A. L. Z.; Voo, Z. X.; Chin, W.; Ono, R. J.; Yang, C.; Gao, S.; Hedrick, J. L.; Yang, Y. Y. Injectable Coacervate Hydrogel for Delivery of Anticancer Drug-Loaded Nanoparticles in Vivo. *ACS Appl. Mater. Interfaces* **2018**, *10* (16), 13274−13282.

(19) Krogstad, D. V.; Lynd, N. A.; Miyajima, D.; Gopez, J.; Hawker, C. J.; Kramer, E. J.; Tirrell, M. V. Structural Evolution of Polyelectrolyte Complex Core Micelles and Ordered-Phase Bulk Materials. *Macromolecules* **2014**, *47* (22), 8026−8032.

(20) Srivastava, S.; Andreev, M.; Levi, A. E.; Goldfeld, D. J.; Mao, J.; Heller, W. T.; Prabhu, V. M.; de Pablo, J. J.; Tirrell, M. V. Gel Phase Formation in Dilute Triblock Copolyelectrolyte Complexes. *Nat. Commun.* **2017**, *8* (1), 14131.

(21) Audus, D. J.; Gopez, J. D.; Krogstad, D. V.; Lynd, N. A.; Kramer, E. J.; Hawker, C. J.; Fredrickson, G. H. Phase Behavior of Electrostatically Complexed Polyelectrolyte Gels Using an Embedded Fluctuation Model. *Soft Matter* **2015**, *11* (6), 1214−1225.

(22) Jiang, J.; Chen, E.-Q.; Yang, S. The Effect of Ion Pairs on Coacervate-Driven Self-Assembly of Block Polyelectrolytes. *J. Chem. Phys.* **2021**, *154* (14), 144903.

(23) Kim, S.; Kim, J.-M.; Wood, K.; Choi, S.-H. Ionic Group-Dependent Structure of Complex Coacervate Hydrogels Formed by ABA Triblock Copolymers. *Soft Matter* **2022**, *18* (21), 4146−4155.

(24) Rahalkar, A.; Wei, G.; Nieuwendaal, R.; Prabhu, V. M.; Srivastava, S.; Levi, A. E.; de Pablo, J. J.; Tirrell, M. V. Effect of Temperature on the Structure and Dynamics of Triblock Polyelectrolyte Gels. *J. Chem. Phys.* **2018**, *149* (16), 163310.

(25) Lemmers, M.; Voets, I. K.; Cohen Stuart, M. A.; van der Gucht, J. Transient Network Topology of Interconnected Polyelectrolyte Complex Micelles. *Soft Matter* **2011**, *7* (4), 1378−1389.

(26) Early, J. T.; Yager, K. G.; Lodge, T. P. Direct Observation of Micelle Fragmentation via In Situ Liquid-Phase Transmission Electron Microscopy. *ACS Macro Lett.* **2020**, *9* (5), 756−761.

(27) Lodge, T. P.; Seitzinger, C. L.; Seeger, S. C.; Yang, S.; Gupta, S.; Dorfman, K. D. Dynamics and Equilibration Mechanisms in Block Copolymer Particles. *ACS Polym. Au* **2022**, *2* (6), 397−416.

(28) Bos, I.; Sprakel, J. Langevin Dynamics Simulations of the Exchange of Complex. *Macromolecules* **2019**, *52*, 8923−8931.

(29) Beaucage, G. Approximations Leading to a Unified Exponential/Power-Law Approach to Small-Angle Scattering. *J. Appl. Crystallogr.* **1995**, *28* (6), 717−728.